JOURNAL OF COMPUTATIONAL PHYSICS **144,** 52–69 (1998)
ARTICLE NO. CP985991

A Front Tracking Method for the Motion of Premixed Flames

J. Qian,* G. Tryggvason,† and C. K. Law*

**Department of Mechanical and Aerospace Engineering, Princeton University, Princeton, New Jersey 08544 and †Department of Mechanical Engineering, The University of Michigan, Ann Arbor, Michigan 48109*

Received February 20, 1997; revised November 11, 1997

A front tracking method to study multi-fluid flows in which a sharp interface separates incompressible fluids of different densities and viscosities is adopted to simulate the unsteady motion of an infinitely thin premixed flame characterized by significant chemical heat release and hence thermal expansion. The flow field is discretized by a conservative finite difference approximation on a stationary grid, and the flame surface is explicitly represented by connected marker points that move with the local flame speed, relative to the flow field. The performance of the method is tested by applying it to a steady planar flame and the Darrieus–Landau instability. The numerical results are in good agreement with analytical results. The method is also applied to the interaction between a flame and a vortex array. The results show that the flame can destroy the vorticity originally in the unburnt gas and generate vorticity of opposite sign in the burnt gas.

1. INTRODUCTION

Propagation of a premixed flame in a turbulent flow is one of the most fundamental and challenging problems in combustion science. A direct numerical simulation of the flow requires the simultaneous solutions of the chemical kinetics coupled with the hydrodynamic equations. The stiffness and nonlinearity of the chemical reaction terms combined with the nonlinearity of the flow makes this an exceedingly difficult task. However, for many practical applications the flame can be treated as a surface of zero thickness moving in a complex flow field. This simplifies the problem considerably, but the task is still fairly challenging.

By treating the flame as a surface, several numerical methods have been developed to simulate the flame motion. One approach is to track a passive flame front by an equation for a scalar field $G(\mathbf{x}, t)$ whose zero level represents the flame. This is the so-called G-equation [1, 2], given by

$$\frac{\partial G}{\partial t} + \mathbf{V}_{G=0} \cdot \nabla G = S_f |\nabla G|, \tag{1}$$

0021-9991/98 $25.00

where $\mathbf{V}$ is the flow velocity and S_f the local normal propagation speed of the flame relative to the unburnt mixture. The G-equation is simply a kinematic description of the propagation of a front in the direction normal to itself, and has been mostly employed for turbulent combustion in the laminar flamelet regime with constant density assumption. Using the G-equation, Peters [3], for example, investigated the flamelet formulation for premixed combustion. By transforming the scaler field equation into wavenumber space, he obtained a definiation of a spectrum function for the turbulent flame front. Aldredge [4] obtained the steady-state flame shapes and the corresponding average flame speeds for periodic flow with different wavelengths, and found that the average flame speed increases with decreasing wavelength of the periodic flow. Aldredge [5] examined the unsteady motion of flames through a prescribed incompressible vortical velocity field, showing that on the average the flame propagation rate increased with the intensity of the vorticity, when the intensity was strong. The recent work by Helenbrook *et al.* [6] on flame and vortex array showed that stretch through curvature effects reduces the mean burning velocity from that obtained by considering only the change in the flame surface area due to flame wrinkling.

Another numerical method, the Simple Line Interface Calculation, or SLIC, originally developed for multifluid flows by Noh and Woddward [7] and Chorin [8], has also been used to describe premixed flames in the unsteady flow fields. In SLIC a marker function is advected with the flow, but explicit reconstruction of the sharp interface during advection prevents numerical diffusion. Wu and Driscoll [9] used the SLIC method to study a pair of vortices convected through a laminar premixed flame with constant density. It was found that a flame cannot propagate over the vortices and thus temporarily remains attached to the moving vortex if the vortex-induced velocity that opposes the flame motion is sufficiently large. The SLIC method was also used by Ashurst and Barr [10] to simulate the interaction between a flame surface and a time dependent turbulent flow. Their results show that the turbulent flame speed is determined from the overall rate of product formation, which depends linearly on the root-mean-square turbulent intensity. The advantages of the SLIC method are that it can include the gas expansion through the flame surface and handle complicated flame topology. However, it is difficult to locate the flame precisely, and hence to evaluate the front curvature, because of the ragged flame in SLIC simulations.

An alternative to capture the flame front by a marker function is to track the front explicitly by either boundary confirming grids or separate computational elements. Unverdi and Tryggvason [11] presented a front tracking method based on marking a boundary between two fluids by connected points. The governing equations for the fluid motion were solved on a fixed grid and the points moved by interpolating velocities from the fixed grid. The density and viscosity of the fluid were reconstructed from the location of the front. The interface is given a small thickness of the order of the mesh size, but this thickness remains constant for all time and therefore numerical diffusion is avoided. This front tracking method has been successfully used to examine several multi-fluid phenomena, including bubbles rising in a gravity field by Esmaeeli and Tryggvason [12] and dendritic solidification of pure substances by Juric and Tryggvason [13]. It has also been used to investigate droplet collisions by Qian *et al.* [14] where it was shown that the calculated results agree well with results obtained through experimental imaging. The formulation used in the method of Unverdi and Tryggvason [11], where one set of conservation equations is solved on a fixed grid, is very similar to the approach taken in the Volume-Of-Fluid method (Hirt and Nichols [15]) and the recently developed level-set-method (Sussman *et al.* [16]) with the exception that Unverdi and Tryggvason [11] explicitly track the interface instead of capturing it with a

marker function. For an application of level-set-methods to flame propagation, see Osher and Sethian [17], where the flame speed was assumed to depend on the flame curvature only and no coupling with the flow field was included.

In this paper we extend the front tracking method of Unverdi and Tryggvason [11] to allow the simulation of the motion of infinitely thin premixed flames. This extension requires us to account for localized expansion at the flame interface where the density changes from that of the unburnt gas to the burnt. Viscosity generally also increases across the flame.

2. NUMERICAL METHOD

The method is an extension of the Unverdi and Tryggvason [11] front tracking technique for multi-fluid flows, following closely some of the ideas presented in Juric and Tryggvason [18] for phase change problems. Figure 1 shows a schematic of the problem. We consider a flame surface propagating through a premixed gas at a flame speed S_f with respect to the unburnt gas. Both the unburnt and the burnt gas are assumed to be incompressible, but expansion takes place as the gas burns upon crossing the flame such that the density of the burnt gas is generally much lower than that of the unburnt gas. Hydrocarbon flames, for example, usually reduce the density of the burnt gas to about one fifth of the unburnt gas under standard atmospheric conditions. Furthermore, viscosities on either side of the flame are constant but unequal, with the viscosity of the burnt gas usually higher than that of the unburnt gas.

Instead of writing the Navier–Stokes equations separately for the burnt and unburnt gas and matching them at the flame, here we write one set of equations that describes the flow in the entire computational domain. Thus, we have to allow for variable density and viscosity fields as well as local expansion across the flame. The Navier–Stokes equations

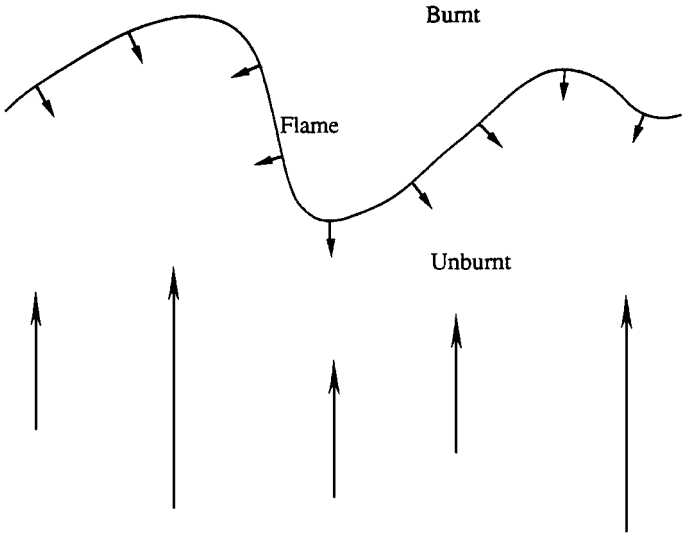

FIG. 1. Schematic of the numerical simulation of the premixed flame propagation in non-uniform flow. The flame separates the burnt and the unburned gas which have different densities and viscosities.

in conservative form are

$$\frac{\partial \rho \mathbf{u}}{\partial t} + \nabla \cdot \rho \mathbf{u}\mathbf{u} = -\nabla p + \nabla \cdot \mu(\nabla \mathbf{u} + \nabla^T \mathbf{u}). \tag{2}$$

Here $\mathbf{u}$ is the velocity field, p the pressure, and ρ and μ are, respectively, the discontinuous density and viscosity fields. The mass conservation equation is

$$\frac{\partial \rho}{\partial t} + \nabla \cdot \rho \mathbf{u} = 0. \tag{3}$$

Away from the flame, the density is constant such that

$$\nabla \cdot \mathbf{u} = 0. \tag{4}$$

Across the flame, however, the divergence of the velocity field is non-zero. The expansion across the flame can be taken into account in several ways, one of which is simply to set the divergence of the velocity field equal to the local rate of expansion. Since the flame is not completely thin in the approach used here as will be explained shortly, we have found it convenient to implement conservation of mass slightly differently from Eq. (4), by working with Eq. (3) directly. Away from the flame where the density is constant it reduces to the usual incompressibility condition (4). At the flame, however, the local rate of change of density is equal to the divergence of the density times the velocity and for a thin flame we can write

$$\nabla \cdot \rho \mathbf{u} = -\int_f \Delta \rho \mathbf{V} \cdot \mathbf{n} \delta(\mathbf{x} - \mathbf{x_f})\, da, \tag{5}$$

where $\mathbf{V}$ is the total velocity of the flame, $\mathbf{n}$ the normal vector, and $\Delta\rho$ the density difference between unburnt and burnt gases. The integration is over the entire flame surface. Adding the delta functions by integrating along the flame results in a source term that is continuous along the flame, but is zero away from the flame. For a detailed derivation of Eq. (5), see the Appendix.

The discretization of these equations is conventional. We use a fixed staggered grid for the velocities and pressure and second order centered differences for all spatial derivatives. Time integration is done by an explicit first order projection method:

$$(\rho \mathbf{u})^* = (\rho \mathbf{u})^n + \Delta t A_h(\mathbf{u}), \tag{6}$$

where $A_h(\mathbf{u})$ is the discretized form of the advection and diffusion term in Eq. (2). The subscripts h and n denote the finite difference approximation for space and time, respectively, and $(\rho \mathbf{u})^*$ is the unprojected mass flux (Peyret and Taylor [19]). The second step is

$$(\rho \mathbf{u})^{n+1} = (\rho \mathbf{u})^* - \Delta t \nabla_h p, \tag{7}$$

where the pressure is found by solving

$$\nabla_h^2 p = \nabla_h \cdot (\rho \mathbf{u})^* - \left(\int_f \Delta \rho (\mathbf{V} \cdot \mathbf{n})^{n+1} \delta(\mathbf{x} - \mathbf{x}_f)\, da \right)_h. \tag{8}$$

Since the total velocity of the flame, $\mathbf{V}$, depends on the pressure, this equation has to be solved in an iterative manner even when there is no expansion at the flame. This pressure equation is slightly different from the usual one for stratified flow because of the manner in which the mass conservation equation is written. It can, however, also be used for sharply stratified flows, in which case $\mathbf{V}$ is simply the fluid velocity, and replaces a pressure equation of variable coefficients with a regular Possion equation where the right hand side depends on the $(n+1)$ time step solution and therefore must be solved iteratively. We solve the pressure equation with a simple SOR iteration (using an over relaxation coefficient of 1.2) and find that generally, only a few iterations of the system (Eqs. (7) and (8)) are required to reach convergence. Here, we compute the error at each grid point and terminate the iteration when the absolute value of the maximum error is smaller than 10^{-4} for the pressure. Pressure is generally $O(1)$ in the computations presented here.

The flame is represented by a "front" consisting of connected points that are advected by velocity interpolated from the fixed grid. This front marks the place where the density and viscosity change values and identifies where the source term in Eq. (5) is located. To transfer the source term, as well as the jump in the density from the front to the fixed grid, we use the smoothing function introduced by Peskin [20]. This results in a discrete approximation to the delta function on the fixed grid that has a width of about 3–4 grid points. To ensure that the front property is conserved as it is smoothed onto the grid we insist that

$$\sum_N \phi_{ij} g_{ij} h^2 = \int_{\Delta s} g_i \, da \tag{9}$$

holds, where N is the number of grid points that the quantity at each front point is distributed to, the ϕ_i's are the weight at each grid point, given by the Peskin interpolation function [20] in our case, g_i is some front quantity, per unit length, and g_{ij} is the same quantity on the fixed grid, per unit volume. Furthermore, h is the grid spacing and we also must have $\sum \phi_{ij} = 1$. We note that since we approximate the delta functions on a fixed grid, we are seeking a "weak" solution that satisfies the correct conservation principles, but is not discontinuous across the flame. The solution to the original partial differential equations should be discontinuous and the transition zone becomes thinner as the grid is refined.

To interpolate the velocity from the grid to the front we also used the Peskin interpolation function. If there is no expansion across the front, the velocity field is continuous and the interpolation is straightforward. Here, however, the fluid velocity is discontinuous across the flame and only the flame speed relative to the unburnt gas, S_f, is given. A straightforward interpolation will yield some approximation of the average velocity, and the value is generally sensitive to the exact location of the front. We have found it more robust to interpolate the mass flux ($\rho\mathbf{u}$) and then divide it by the average density to get the average local fluid velocity, $\mathbf{u}_{av}$. Once the average fluid velocity has been found by interpolation, the total flame velocity is obtained as

$$\mathbf{V}_f = \mathbf{u}_{av} + S_{f,av}\mathbf{n}, \qquad \text{with } S_{f,av} = S_f \rho_u/(\rho_u + \rho_b), \tag{10}$$

where $S_{f,av}$ is the flame speed relative to the local average fluid velocity $\mathbf{u}_{av}$; ρ_u and ρ_b are the densities of unburnt and burnt gases. Once the velocity of the front points is found, a new position is computed by a first order explicit time integration. We note that although we have used a first order scheme here for both the field equations and the front advection,

we believe that it is relatively easy to implement a second order method along the line of the predictor-corrector method used by Esmaeeli and Tryggvason [12], for example. The size of the time step is selected by using the usual restrictions for centered difference schemes with explicit time integration (Peyret and Taylor [19]). Based on our experience with multifluid flows without any reaction at the interface we believe that either different advection schemes or different spacial differentiation could be used, without affecting the basic performance of the method.

One additional difficulty arises due to the finite thickness of the transition zone from the burnt to the unburnt gas. The divergence of the velocity field is non-zero in a zone of finite thickness around the flame, and this results in a normal stress that is balanced by a local pressure peak. To avoid this peak we redefine the pressure by explicitly subtracting $2\mu(\nabla \cdot \mathbf{u})\,\mathbf{I}$ from the stresses (see Juric and Tryggvason [18]). This redefinition has no effect on the results, but does make the average of the diagonal terms in the stress tensor equal to the pressure, as it is for incompressible flows.

All simulations were performed on workstations. The run in Subsection 3.3 on a 140 by 280 grid took about 8 hours on a DEC 3000.

3. COMPUTATIONAL EXAMPLES

3.1. *One-Dimensional Flame*

We first show numerical results for a steady state one-dimensional flame with a uniform inflow of reactants ($u = 1$ and $\rho = 1$ at $x \to -\infty$). The analytical solutions for density ρ, velocity u, and pressure p are

$$\begin{cases} \rho = 1, & u = 1, & \text{and} & p = q - 1,\ x < 0 \\ \rho = 1/q, & u = q, & \text{and} & p = 0,\ x > 0 \end{cases} \tag{11}$$

with the flame located at $x = 0$, where q is the ratio of the densities of the unburnt and burnt gas. The mass flux ρu and the total pressure $(p + \rho u^2)$ are constant. The flame speed is $S_f = 1$ with respect to the unburned gas, the viscosity of both the unburned and burned gas is 0.005, and the size of the computational domain is 1 by 1. At the inlet the velocity and density is specified and at the outlet the velocity gradient is set to zero.

Figures 2 and 3 show the profiles of ρ, u, ρu, and p across the flame for two different grid resolutions: 20 and 40 grid points in a unit domain, respectively. It is seen that the density decreases and the velocity increases across the flame, while the mass flux ρu is constant. The pressure decreases and the reactant is burned and expanded through the flame, while the total pressure $(p + \rho u^2)$ is constant in the entire domain. These results clearly show that the computed transition zone jump becomes sharper with increasing grid resolution and approaches the analytical results. We note that ρu is only constant for stationary flames and for moving flames we expect a larger uncertainty in the determination of the flame velocity.

3.2. *Computation of Darrieus–Landau Instability*

We next use the front tracking method to study the Darrieus–Landau instability [21]. To compute the linear growth rates, we take as the initial condition a flame in the shape of a sine wave of a low amplitude (10^{-2} in units of wave length). The physical parameters are

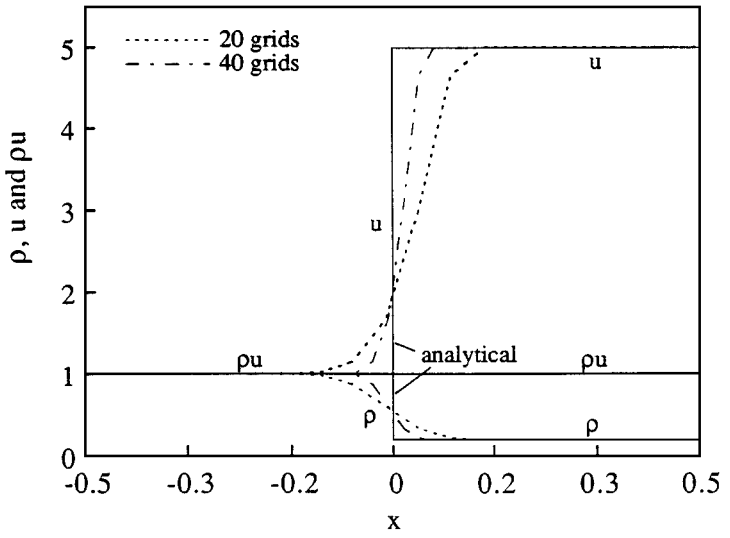

FIG. 2. A comparison of numerically computed density, velocity, and mass flux in a one dimension steady-state flame with analytical results. Results for two different grids, with 20 and 40 grid points, are shown.

$\rho_u = 1.0$, $\rho_b = 0.2$, $\mu_u = 0.011$, $\mu_b = 0.035$, and $S_f = 1$. These numbers have been selected to give nondimensional numbers similar to a methane flame at atmospheric conditions. The computational domain is a square with side lengths equal to $2\pi/5$ and resolved by 60 by 60 grid points. After a short initial transient, the amplitude begins to grow exponentially. Figure 4(a) shows the flame instability development for small sinusoidal disturbance of wave number 5 with a density ratio of 5; Fig. 4(b) plots the logarithm of the amplitude normalized by the initial amplitude as a function of time for density ratios of 3, 4, and 5. For the smaller density ratio the density of the burned gas is increased, but other parameters are unchanged. There is a good agreement between the numerical and the analytical results.

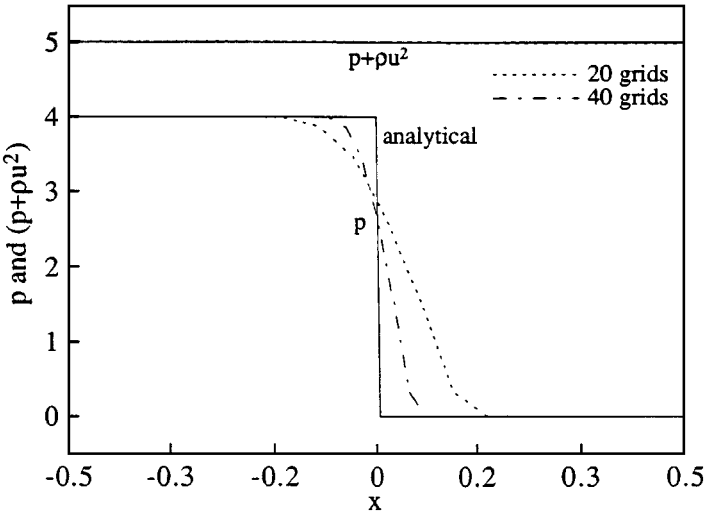

FIG. 3. A comparison of numerically computed pressure in a one dimension steady-state flame with analytical results. Results for two different grids, with 20 and 40 grid points, are shown.

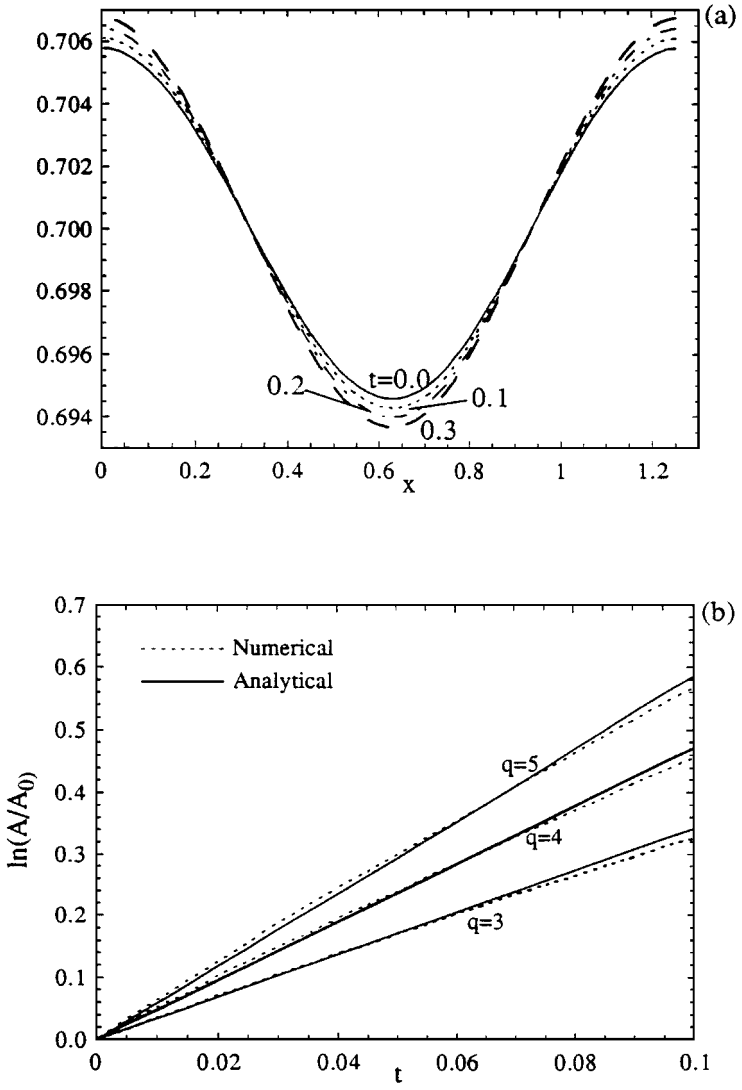

FIG. 4. (a) The development of a Darrieus–Landau flame instability from a small sinusoidal disturbance of wave number 5 with density ratio of 5; (b) comparison between the computed growth and analytical results for wave number 5 and three different density ratios.

Note that the amplitude growth is reduced in the numerical results as time increases due to nonlinear effects [22]. While the finite size of the computational domain may also contribute to the reduction in the growth rate, we believe the effects are small for the small amplitude that we are examining here.

The development of the instability for larger disturbances with nonlinear effects is shown in Fig. 5. The initial flame is again a sinusoidal shape with wave number 5 and amplitude 0.2. The relatively large amplitude was selected to avoid the appearance of short waves that contaminate the solution in Fig. 4 at late times. These waves are triggered by the grid and are a consequence of the ill-posedness of the flame problem when no short wave stabilization mechanism is included. In the computation presented in the next section, we introduce a Markstein length to stabilize those short waves. The instability develops quickly, resulting in an unsymmetric flame front with a typical cusp pointing towards the burnt gas as often seen

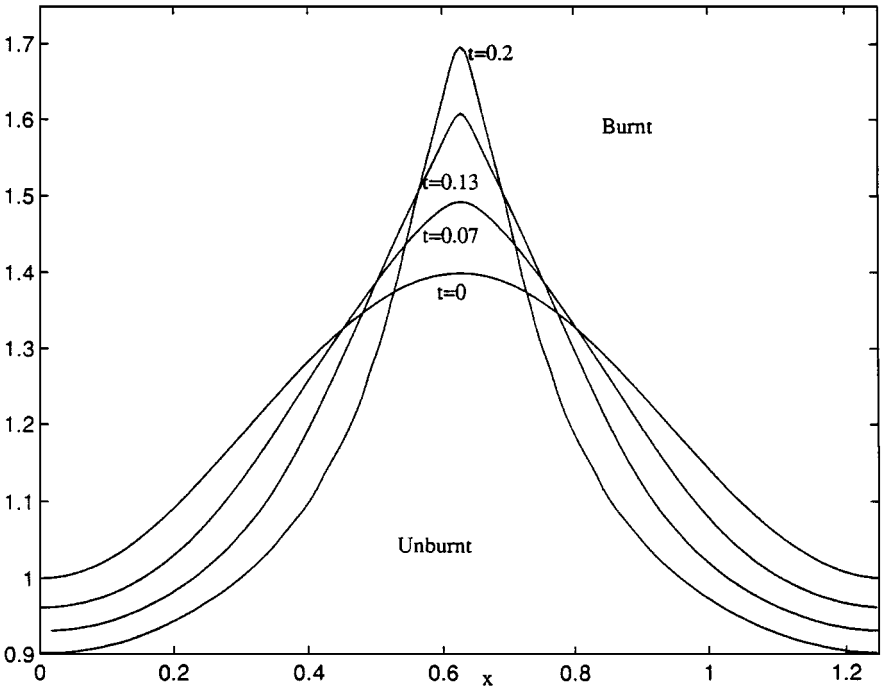

FIG. 5. The nonlinear evolution of a Darrieus–Landau flame instability for wave number 5 and initial disturbance amplitude of 0.2. A cusp pointing towards the burnt gas, as often seen in premixed flames, is formed.

in premixed flames. Due to the conservation of normal mass flux and transverse velocity, the pressure near the cusp is lower than that at the flame trough. The gas flow converges when it moves toward the cusp in the unburnt region, then diverges from the flame in the burnt region due to the expansion, as shown in Fig. 6.

We have repeated the computation of the initial evolution of the instability on different grids and found it to be essentially unchanged for grids with as few as eight grid points per wave length. The insensitivity to the resolution is presumably due to the fact that the flame velocity is specified and the growth of the initial wave is due to its geometry, rather than hydrodynamic effects. A more demanding test problem, where the generation of vorticity at the flame front and its subsequent evolution must be accounted for is presented in the next section.

3.3. *Flame Propagation in a Vortical Flow Field*

We next apply the front tracking method to study the coupling between gas expansion and hydrodynamics by simulating the interaction of a flame with an already existing vorticity field. At time zero the vorticity is assumed to consist of an array of Oseen vorticies. For a single Oseen vortex, the vorticity strength decreases exponentially from the vortex center, and the azimuthal velocity in polar coordinate is given by

$$V_\theta = \frac{\Gamma}{2\pi r}[1 - \exp(-r^2/R^2)], \tag{12}$$

where R is the vortex core size and Γ is the total circulation. Here we take $R = 0.5$ and $\Gamma = 1.5$ so the maximum velocity induced by the vortex is $V_{\theta,m} = 0.25$. The period length of the vortex array is 5. To suppress the hydrodynamic instability development at

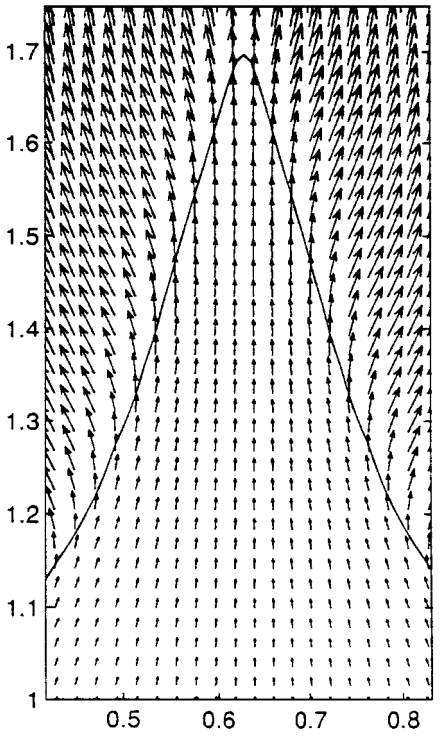

FIG. 6. Velocity vectors around the cusp formed at late times. The flow in the unburned gas converges toward the cusp, then diverges from the flame in the burnt region due to the expansion when the fluid crosses the flame.

short wavelengths, we use a Markstein length parameter in the flame speed expression, $S_f = S_{f,0}(1 + L\kappa)$, where L is the Markstein number [23, 24] and κ is the curvature of the flame. The computation was performed in a rectangular domain of width 5 (one period length in the x direction) and length 10 (in the y direction), and resolved by 140 by 280 grid points. The density ratio is 5 and $L = 0.1$. L was selected in such a way that small scale waves were stabilized, but the effect on longer waves was minimal. Other physical parameters are the same as in the last section.

The evolution of the flame front through the vortex is shown in Fig. 7. The flame speed is directed downward, but as the flame moves through the vortex it is distorted. To investigate how much of the distortion is due to the velocity induced by the vortex and how much is due to the local expansion in the flame, we have also computed the motion of a flame with the same velocity, relative to the unburnt gas, but assuming no expansion so the densities in the burnt gas are the same as those in the unburnt one. Since there is no expansion at the interface, decay of the initial vorticity is by diffusion only. The evolution of the flame for this case is shown in Fig. 8, and it is seen that while the flame is not flat, the deformation is much smaller than when there is expansion across the flame. Thus, while the presence of the vortex disturbs the flame, the subsequent evolution is due to a Landau instability of the perturbed interface. Since the vortex induces a counterclockwise rotational velocity in the fluid, the flame is pushed down to the left of the vortex and up on the right hand side. Once the flame passes the vortex, it moves to the right with the fluid. Since we have modified the flame speed to stabilize short wave perturbations, the spike protruding upward has a rounded “nose” that moves down with the flame.

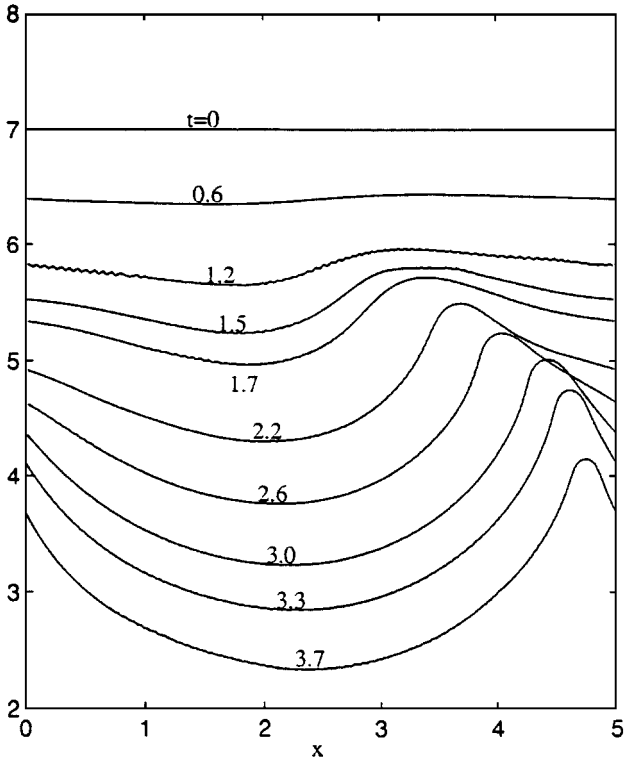

FIG. 7. The evolution of the flame front as it moves over a stationary vortex. Here the density between the unburned and the burned gas is 5.

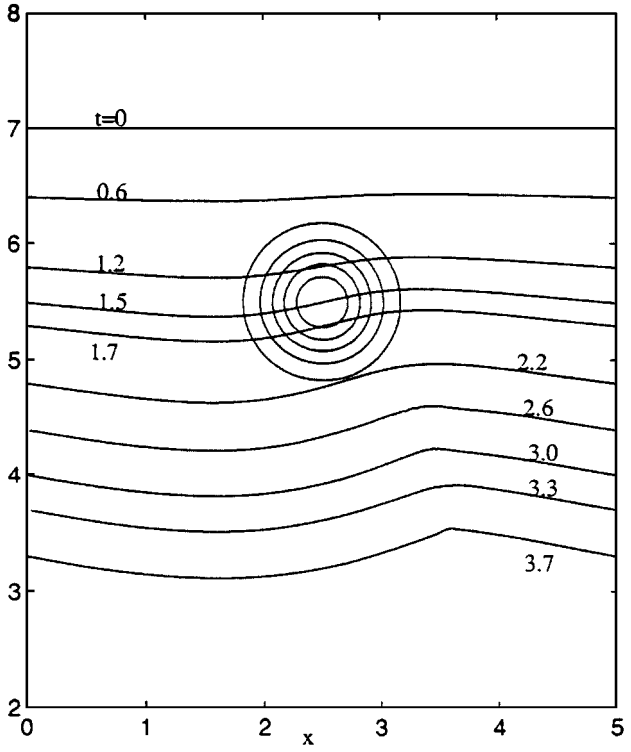

FIG. 8. The evolution of the flame front as it moves over a stationary vortex. Here there is no expansion in the flame and the density in the unburned and the burned gas are the same.

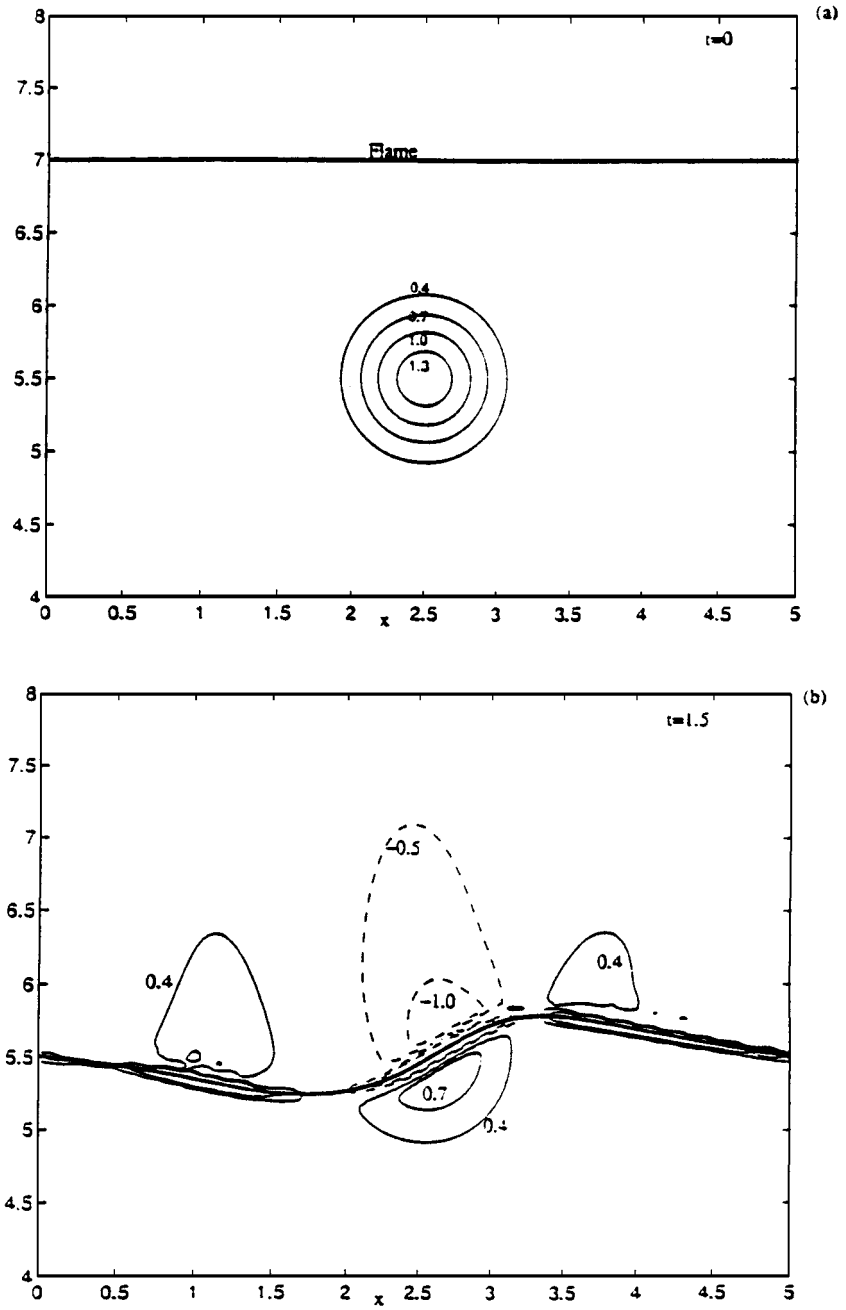

FIG. 9. Generation and attenuation of vorticity by the passage of a flame through an initially stationary vortex. The flame and the vorticity field are shown at times $t = 0$, 1.5, and 1.9. The initial radially symmetric vorticity configuration is destroyed, and new vorticity corresponding to the deformed flame is generated.

The flame and the vorticity contours at $t = 0$, 1.5, and 1.9, are shown in Figs. 9(a)–9(c). Initially, the only vorticity is in the vortex, but as the flame moves downward, secondary vorticity appears behind the flame. The vorticity is negative where the flame has a positive slope and positive where the flame slope is negative. Since there is a strong upward velocity above the flame due to the expansion across the flame, the vorticity is carried upward. We note that there are no remains of the original positive vorticity in the middle of the

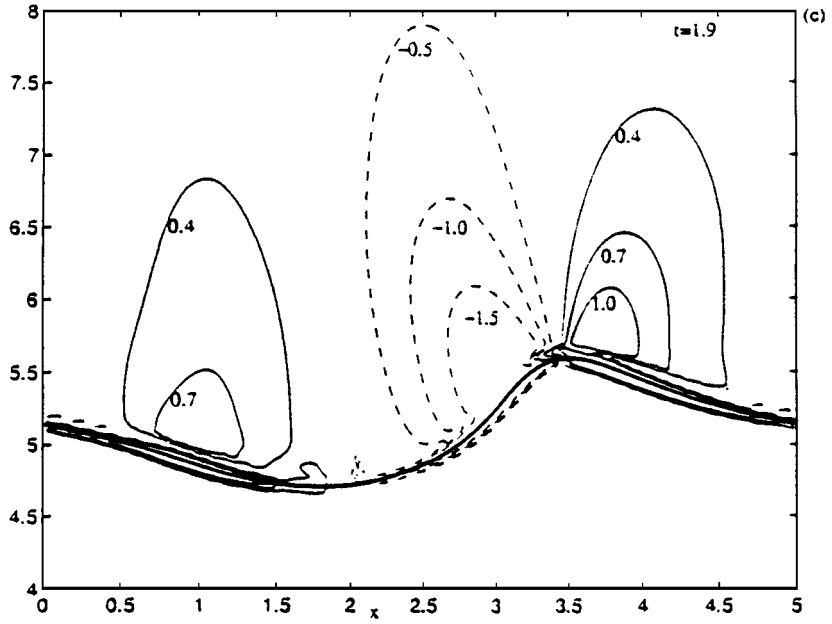

FIG. 9—*Continued*

domain once the flame has passed ($t = 1.9$), and that the strength of the secondary vorticity is comparable with that of the original vortex. These results demonstrate the significant influence of gas expansion across a flame on the hydrodynamics, and the necessity of taking into account the coupling between the flame and the flow field.

To demonstrate that the results in Figs. 7 and 9 are well converged, we compare the solutions at $t = 1.9$ for the flame front and vorticity contours, as calculated on three different grids. Figure 10 shows the flame shape, and Fig. 11 shows the vorticity contours for three

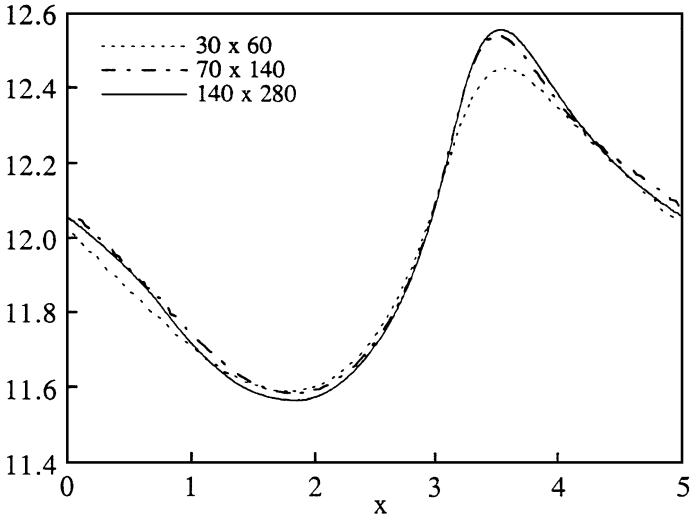

FIG. 10. Resolution test for the flame front at $t = 1.9$. The results from three grid resolutions are shown: 30 by 60, 70 by 140, and 140 by 280. As the grid is refined, the flame shape converges.

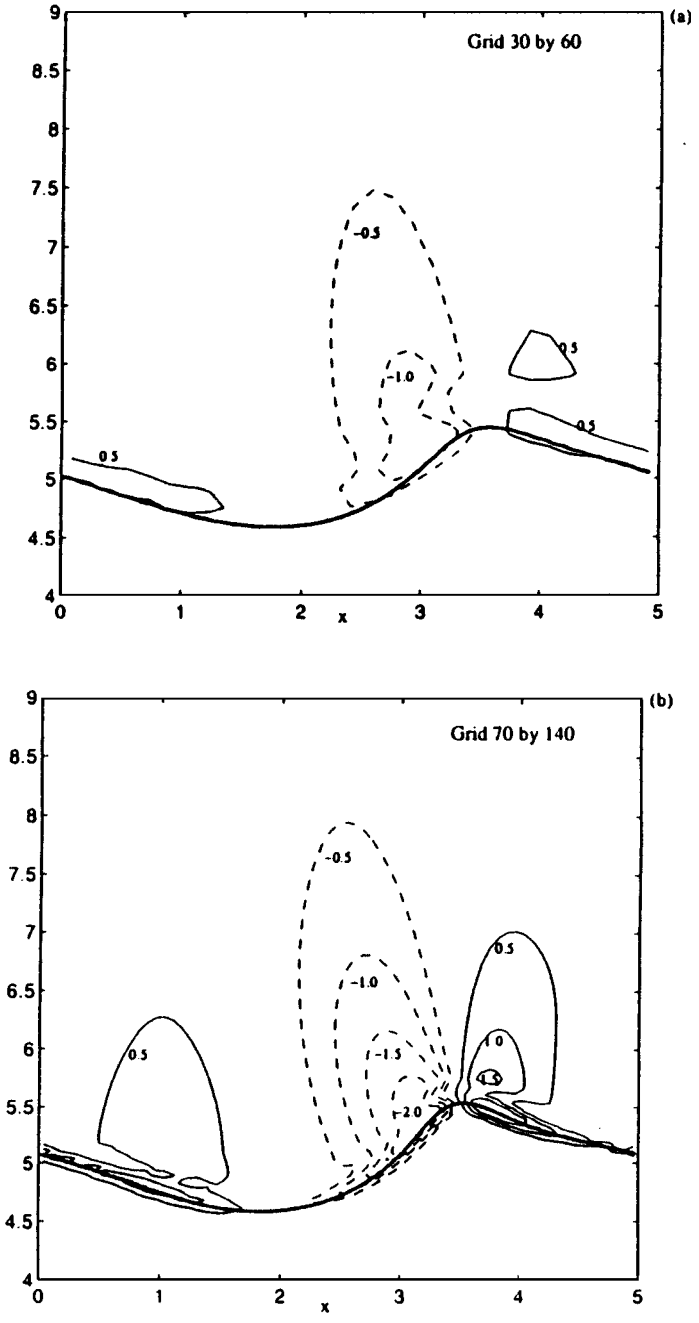

FIG. 11. Resolution test showing the vorticity contours at $t = 1.9$ for three grid resolutions: 30 by 60, 70 by 140, and 140 by 280. As the grid is refined, the vorticity contours converge. Notice that the contour levels have been selected slightly differently than in Fig. 9 to show the shape of the vorticity distribution on the coarser grids better.

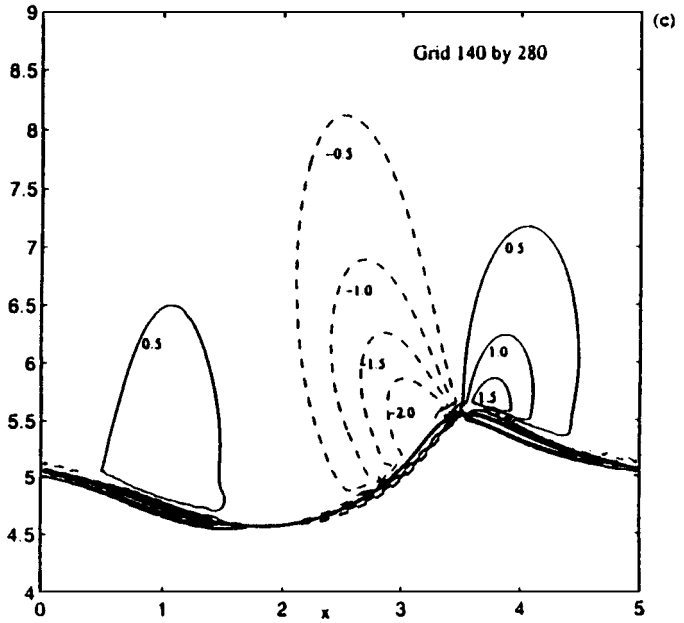

FIG. 11—*Continued*

different grid resolutions: 30 by 60, 70 by 140, and 140 by 280 grid points. Notice that the contour levels have been selected slightly different than in Fig. 9 to show the shape of the vorticity distribution on the coarser grids better. The flame fronts are close for different grids, and the vorticity contours become similar as the grids become finer.

4. CONCLUSIONS

A numerical method for the simulation of the unsteady motion of a premixed flame has been presented. The flame is assumed to be a surface separating the burnt and unburnt gas, propagating with a prescribed flame velocity. The density and other material properties change discontinuously across the flame. The Navier–Stokes equations are solved on a stationary two-dimensional finite difference grid for both the unburnt and the burnt gas, and the flame surface is explicitly tracked by connected marker points.

The accuracy of the method has been demonstrated by comparison of the results with exact solutions for a one-dimensional steady flame and the Darrieus–Landau instability, and through grid resolution studies. The method has also been applied to the interaction of a flame with a vortex array. The results show both wrinkling of the flame and the appearance of flame-generated vorticity in the burnt gas.

The major limitation of the method as currently implemented is the thin flame assumption and hence the inability to resolve the diffusive structure of the flame by solving for the energy and the species diffusion equations. While direct simulations where all details of the flow and the chemical reaction field are resolved are starting to appear (see Poinsot *et al.* [25] for a simulation of the interaction of a vortex with a premixed flame, and Denet and Haldenwang [26] for a simulation of the Darrieus–Landau instability) such simulations are limited to a relatively small range of scales. It is likely that that a more complete flame model (such as the one presented by Dahm *et al.* [27] for a strained diffusion flame) could be incorporated

into the present methodology to account for the diffusive structure (which would allow new effects such as quenching) without increasing the resolution requirement significantly.

APPENDIX

The density can be written in terms of the constant densities on either side of the interface and a Heaviside function, H, which is unity in fluid i and zero in fluid o:

$$\rho(x, y, t) = \rho_i H(x, y, t) + \rho_o(1 - H(x, y, t)).$$

Here we have assumed a two-dimensional flow. The extension to three-dimensions is straight forward. The time derivative of the density is

$$\frac{\partial \rho}{\partial t} = \rho_i \frac{\partial H}{\partial t} - \rho_o \frac{\partial H}{\partial t} = (\rho_i - \rho_o)\frac{\partial H}{\partial t}.$$

To find the time derivative of the Heaviside function, it is perhaps most convenient to express H in terms of an integral over the product of one-dimensional δ-functions:

$$H(x, y, t) = -\oint_{A(t)} \delta(x - x')\,\delta(y - y')\mathbf{n}\, ds.$$

The integral is over an area A bounded by a contour S. H is obviously 1 if (x, y) is within S and 0 otherwise. To find the time derivative of H, note that since H is either 1 or 0, its evolution is governed by

$$\frac{\partial H}{\partial t} + \mathbf{V} \cdot \nabla H = 0,$$

where $\mathbf{V}$ is a smooth velocity field that matches the interface velocity at the interface (if there is no expansion at the interface and the fluids are incompressible, $\mathbf{V}$ could be the fluid velocity). To find the gradient of H we note first that since the gradient is with respect to the unprimed variables, the gradient operator can be put under the integral sign. Since the δ-functions are anti-symmetric with respect to the primed and unprimed variables, the gradient with respect to the unprimed variables can be replaced by the gradient with respect to the primed variables. The resulting volume (or area in two-dimensions) integral can then be transformed into a surface (line) integral by a variation of the divergence theorem for gradients. Symbolically,

$$\begin{aligned}\nabla H &= \int \nabla(\delta(x - x')\,\delta(y - y'))\, da' = -\int \nabla'(\delta(x - x')\,\delta(y - y'))\, da' \\ &= -\oint \delta(x - x')\,\delta(y - y')\mathbf{n}\, ds,\end{aligned}$$

where the prime on the gradient symbol denotes the gradient with respect to the primed variables. The velocity field is smooth and a function of the unprimed variables, so we can bring it under the integral sign, resulting in

$$\frac{\partial H}{\partial t} = -\mathbf{V} \cdot \nabla H = -\oint_S \delta(x - x')\,\delta(y - y')V_n\, ds,$$

where $V_n = \mathbf{V} \cdot \mathbf{n}$. Since the density jump is constant, this leads to

$$\frac{\partial \rho}{\partial t} = \oint_S \Delta\rho \delta(x - x')\,\delta(y - y') V_n\, ds,$$

where we have put $\Delta\rho = \rho_o - \rho_i$. Rewriting the mass conservation equation as

$$\nabla \cdot \rho \mathbf{u} = -\frac{\partial \rho}{\partial t}$$

and replacing the right hand side by the expression above yields Eq. (5) in the paper. Here, we have assumed that the area occupied by the other fluid is finite so that S is a closed contour. Since the contribution of most of the integral is zero, we can replace it by one over a part of the contour and drop the circle on the integral.

ACKNOWLEDGMENTS

The research at Princeton University and the University of the Michigan were respectively supported by the Air Force Office of Scientific Research and by the National Science Foundation. We thank Dr. D. Juric for many helpful discussions during the course of this work.

REFERENCES

1. A. R. Kerstein, W. T. Ashurst, and F. A. Williams, Field equation for interface propagation in an unsteady homogeneous flow field, *Phys. Rev. A* **37**, 2728 (1988).
2. W. T. Ashurst, G. I. Sivashinsky, and V. Yakhot, Flame front propagation in unsteady hydrodynamic flow, *Combust. Sci. Tech.* **62**, 273 (1988).
3. N. Peters, A spectral closure for premixed turbulent combustion in the flamelet regime, *J. Fluid Mech.* **242**, 611 (1992).
4. R. C. Aldredge, The propagation of wrinkled premixed flame in a spatially periodic shear flow, *Combust. Flame* **90**, 121 (1992).
5. R. C. Aldredge, Premixed flame propagation in a high-intensity, large-scale vortical flow, *Combust. Flame* **106**, 29 (1996).
6. B. T. Helenbrook, C. J. Sun, C. K. Law, and W. T. Ashurst, On stretch-affected flame propagation in vortical flows, *Combust. Flame* **104**, 460 (1996).
7. W. Noh and P. Woodward, Simple line interface calculation, in *Proceedings of the Fifth International Conference on Numerical Methods in Fluid Dynamics*, edited by A. I. Vooren and P. J. Zanbergen (Springer-Verlag, Berlin, 1976), p. 330.
8. A. J. Chorin, Flame advection and propagation algorithms, *J. Comput. Phys.* **35**, 1 (1980).
9. M. S. Wu and J. F. Driscoll, A numerical simulation of vortex convected through a laminar premixed flame, *Combust. Sci. Tech.* **91**, 310 (1991).
10. W. T. Ashurst and P. K. Barr, Stochastic calculation of laminar wrinkled flame propagation via vortex dynamics, *Combust. Sci. Tech.* **34**, 227 (1983).
11. S. O. Unverdi and G. Tryggvason, A front tracking method for viscous incompressible flows, *J. Comput. Phys.* **100**, 25 (1992).
12. A. Esmaeeli and G. Tryggvason, An inverse energy cascade in two-dimensional, low Reynolds number bubbly flows, *J. Fluid Mech.* **314**, 315–330 (1996).
13. D. Juric and G. Tryggvason, A front tracking method for dentritic solidification, *J. Comput. Phys.* **123**, 127 (1996).
14. J. Qian, G. Tryggvason, and C. K. Law, *An Experimental and Computational Study of Bouncing and Deformation in Droplet Collision*, AIAA Paper No. 97-0129, 1997.

15. C. W. Hirt and B. D. Nichols, Volume of fluid (VOF) method for the dynamics of free boundaries, *J. Comput. Phys.* **39**, 201 (1981).
16. M. Sussman, P. Smereka, and S. Osher, A level set approach for computing solutions to incompressible two-phase flow, *J. Comput. Phys.* **114**, 146 (1994).
17. S. Osher and J. A. Sethian, Fronts propagating with curvature-dependent speed: Algorithms based on Hamilton–Jacobi formulations, *J. Comput. Phys.* **79**, 12 (1988).
18. D. Juric and G. Tryggvason, Computations of boiling flows, *Int. J. Multiphase Flow*, in press.
19. R. Peyret and T. D. Taylor, *Computational Methods for Fluid Flows* (Springer-Verlag, New York/Berlin, 1983).
20. C. S. Peskin, Numerical analysis of blood flow in the heart, *J. Comput. Phys.* **25**, 220 (1977).
21. L. D. Landau and E. M. Lifshitz, *Fluid Mechanics* (Pergamon, Elmsford, NY, 1959).
22. G. I. Sivashinsky, Nonlinear analysis of hydrodynamic instability in laminar flames. I. Derivation of basic equations, *Acta Astronautica* **4**, 1177 (1977).
23. P. Pelce and P. Clavin, Influence of hydrodynamics and diffusion upon the instability limits of a laminar premixed flames, *J. Fluid Mech.* **124**, 219 (1982).
24. C. K. Law, Dynamics of stretched flames, in *Twenty-Second Symposium (International) on Combustion* (The Combustion Institute, Pittsburgh, 1988), p. 1381.
25. T. Poinsot, D. Veynante, and S. Candel, Quenching processes and premixed turbulent combustion diagrams, *J. Fluid Mech.* **228**, 561 (1991).
26. B. Denet and P. Haldenwang, A numerical study of premixed flames Darrieus–Landau instability, *Combust. Sci. Tech.* **104**, 143 (1995).
27. W. J. A. Dahm, G. Tryggvason, and M. Zhuang, Integral method solution of time-dependent strained diffusion-reaction equations with multi-step kinetics, *SIAM J. Appl. Math.* **56**, 1039 (1996).